2019

Air-soil diffusive exchange of PAHs in an urban park of Shanghai based on polyethylene passive sampling: Vertical distribution, vegetation influence and diffusive flux

Ying Liu

Shuya Xie

Lirong Zheng

Tongtong Li

Yajie Sun

Citation/Publisher Attribution

Liu, Ying; Xie, Shuya; Zheng, Lirong; Li, Tongtong; Sun, Yajie; Ma, Limin; Lin, Zhifen; Grathwohl, Peter; Lohmann, Rainer. Air-soil Diffusive Exchange of PAHs in an Urban Park of Shanghai Based on Polyethylene Passive Sampling: Vertical Distribution, Vegetation Influence and Diffusive Flux. *Sci Tot Environ* **2019**, 689, 734-742. doi: 10.1016/j.scitotenv.2019.06.500

Available at: https://doi.org/10.1016/j.scitotenv.2019.06.500

Air-soil Diffusive Exchange of PAHs in an Urban Park of Shanghai Based on Polyethylene Passive Sampling: Vertical Distribution, Vegetation Influence and Diffusive Flux

YING LIU[†,‡,*], SHUYA XIE[†,‡], LIRONG ZHENG[ϕ,†], TONGTONG LI[†], YAJIE SUN[†], LIMIN MA[†], ZHIFEN LIN[#], PETER GRATHWOHL[§], RAINER LOHMANN[||]

[†] *State Key Laboratory of Pollution Control and Resource Reuse, College of Environmental Science and Engineering, Tongji University, 1239 Siping Road, Shanghai 200092, China*

[‡] *China Meteorological Administration Key Laboratory of Cities' Mitigation and Adaptation to Climate Change (Shanghai Meteorological Bureau), IESD, Tongji University, Shanghai 200092, China*

[ϕ] *Shanghai Shangde Experimental School, 1688 Xiuyan Road, Shanghai 200092, China*

[#] *Shanghai Key Lab of Chemical Assessment and Sustainability, College of Environmental Science and Engineering, Tongji University, 1239 Siping Road, Shanghai 200092, China*

[§] *Center for Applied Geoscience, University of Tübingen, Hölderlinstrasse 12, 72074 Tübingen, Germany*

[||] *Graduate School of Oceanography, University of Rhode Island, Narragansett, Rhode Island 02882-1197, United States.*

* To whom correspondence should be addressed

E-mail address: liu_ying@tongji.edu.cn (Y. Liu)

29

30

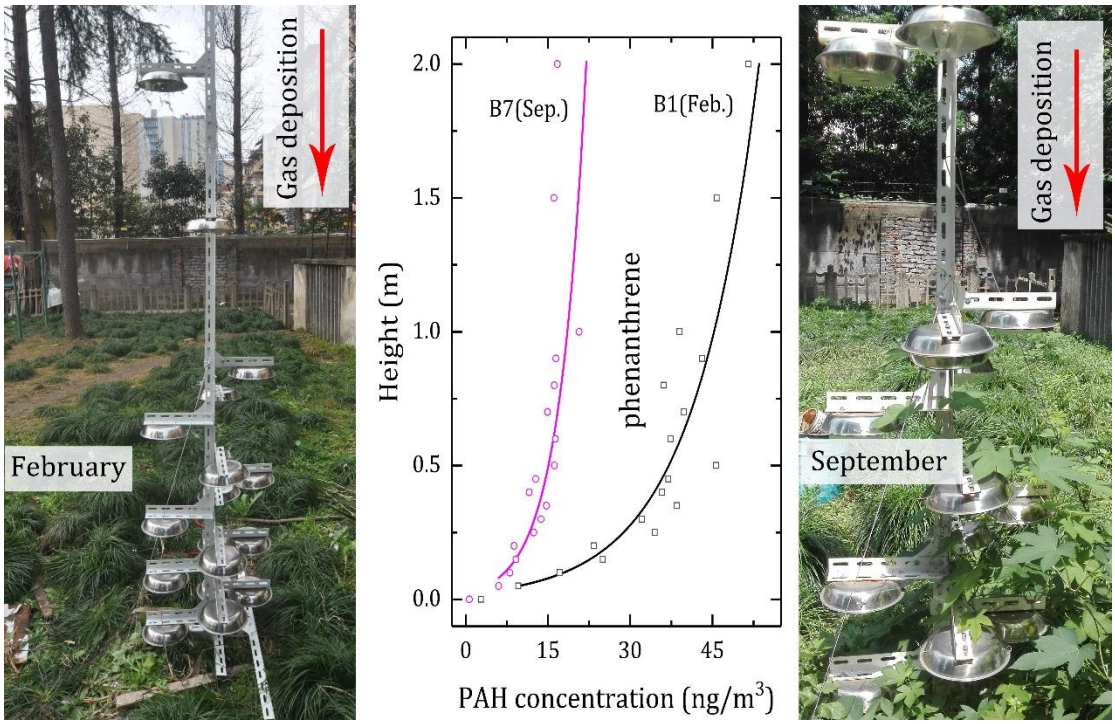
Gas deposition
February
B7(Sep.)
B1(Feb.)
phenanthrene
Height (m)
2.0
1.5
1.0
0.5
0.0
0
15
30
45
PAH concentration (ng/m3)
Gas deposition
September

31

32

HIGHLIGHTS

- Gas deposition for phenanthrene and volatilization for benzo[*b*]fluoranthene.
- Impact of vegetation on vertical pattern of PAHs was observed only in growing season.
- Vertical eddy diffusivity in air was calculated by local micrometeorological conditions.
- Diffusive flux of gaseous PAHs in air-soil exchange was compared from two approaches.

ABSTRACT:

Compared with dry and wet deposition rates, air-soil exchange fluxes cannot be directly measured experimentally. Polyethylene passive sampling was applied to assess transport directions and to measure concentration gradients in order to calculate diffusive fluxes of polycyclic aromatic hydrocarbons (PAHs) across the air-soil interface in an urban park of Shanghai, China. Seven campaigns with high spatial resolution sampling at 18 heights between 0 and 200 cm above the ground were conducted in 2017 - 2018. Air-to-soil deposition was observed, e.g. for phenanthrene, and soil-to-air volatilization for high molecular weight compounds, such as benzo[*b*]fluoranthene. Significant linear correlations between gaseous PAH concentration and log-transformed height were observed. Influence of vegetation on vertical concentration gradients of gaseous PAHs was insignificant in most cases except during the growing season. Local micrometeorological conditions resulted in a directional eddy diffusion in air and then influenced vertical diffusion of gaseous PAHs. Furthermore, the vertical eddy diffusivity was estimated as a function of distance to the air-soil surface. Air-soil exchange fluxes based on the Mackay's fugacity approach were calculated and confirmed by diffusive fluxes within air layer based on vertical concentration gradient of PAHs and eddy/molecular diffusion. Polyethylene passive sampling technology provides a useful tool to investigate air-soil exchange process.

KEYWORDS:

LDPE, gas exchange, eddy diffusion, molecular diffusion, fugacity, uncertainty analysis.

64

65 **1. INTRODUCTION**

66 Polycyclic aromatic hydrocarbons (PAHs) are a ubiquitous class of semi-volatile
67 organic pollutants mainly originating from the combustion of organic matter and
68 fuels (Liu et al., 2015), and are widespread all over the world (Casal et al., 2018).
69 Consequently, the earth surface (e.g. soil and vegetation) becomes a critical sink
70 of these hydrophobic pollutants via atmospheric deposition and direct
71 application e.g. by sewage sludge (Feng et al., 2017; Zheng et al., 2015). After
72 primary pollutant sources were reduced or eliminated in air, soils may become
73 secondary sources of accumulated semi-volatile organic compounds depending
74 on air-surface exchange rates (Bao et al., 2015; Degrendele et al., 2016).

75 To assess air-soil exchange, many studies quantified gradients in air and soil
76 fugacities based on model predictions or field measurements. The latter include
77 active air sampling (e.g. low-volume air samplers) (Degrendele et al., 2016; Kurt-
78 Karakus et al., 2006; Tasdemir et al., 2012; Wang et al., 2015) and more recently
79 passive sampling technologies to measure the air fugacity based on polyurethane
80 foam, low-density polyethylene (LDPE) and other materials (Donald and
81 Anderson, 2017; Dumanoglu et al., 2017; Wang et al., 2017; Zhang et al., 2011).
82 Also, concentrations measured in soil samples were converted to fugacities based
83 on air-soil partitioning coefficients and ambient temperatures (Cetin et al.,
84 2017a; Cetin et al., 2019; Qu et al., 2019; Tasdemir et al., 2012; Wang et al., 2017;
85 Zhang et al., 2011). However, large uncertainties exit in estimating air-soil
86 partitioning coefficients and because of soil heterogeneity, e.g. during soil
87 sampling vertical concentration gradients are disturbed leading to
88 misinterpretation on soil fugacity (Ali et al., 2015; Davie-Martin et al., 2015;

89 Donald and Anderson, 2017). Alternative in situ technologies have been
90 developed to directly monitor the soil air, namely the gas phase in soil pores. For
91 example, active fugacity samplers were designed to sample the air close to the
92 soil surface (Cabrerizo et al., 2009; Degrendele et al., 2016; Wang et al., 2015).
93 Donald and Anderson (2017) designed a soil air fugacity sampler based on
94 passive sampling using polyethylene. In addition to assessing the fugacity
95 gradient between soil and air phases, vertical concentration gradients in air can
96 serve as an alternative indicator and reflect the driving force of the air-soil
97 exchange. For example, Kurt-Karakus et al. (2006) mounted active air samplers at
98 the heights of 5, 20, 72, and 200 cm above ground. Lammel et al. (2011) also
99 actively collected air samples from 1.1 and 2.3 m above the soil surface. To not
100 disturb the atmospheric concentration gradients caused by active sampling,
101 Zhang et al. (2011) and Wang et al. (2017) deployed PUF air passive samplers at
102 various heights above the surface.
103 Many studies focused only on assessing transport direction of air-soil diffusive
104 exchange based on fugacity ratio of air and soil (Cetin et al., 2017a; Cetin et al.,
105 2017b; Degrendele et al., 2016; Tian et al., 2016; Wang et al., 2015; Zhu et al.,
106 2017). However, only in few studies exchange fluxes were calculated based on
107 fugacity gradients between soil and air, following the Mackay fugacity approach
108 (Koblizkova et al., 2009; Pokhrel et al., 2018; Tasdemir et al., 2012; Wang et al.,
109 2017; Zhang et al., 2011) or Fick's law of diffusion (Donald and Anderson, 2017).
110 If the influence of vegetation on air-soil is negligible, the diffusive flux within air
111 layer overlying the soil surface would be equal to the air-soil diffusive exchange
112 rates. This prompted us to deploy more passive samplers with high spatial
113 resolution in the topsoil and air at various heights above ground, in order to

estimate and compare the diffusive fluxes from the two methods. Low density polyethylene (LDPE) passive samplers were placed in heights of 5 - 200 cm above the soil surface during 2017 - 2018. The objectives of this study were to (a) investigate vertical distribution of gaseous PAHs within air phase and determine their transport direction in air-soil exchange process, (b) assess influence of vegetation on the vertical distribution of gaseous PAHs, (c) quantify eddy diffusivities and estimate diffusive fluxes of gaseous PAHs at different heights above the surface based on local micrometeorological conditions, and (d) compare diffusive fluxes within air phase and in the air-soil exchange interface.

2. MATERIALS AND METHODS

2.1 Study site.

The monitoring site was located in a green space in the city center of Shanghai, China, ~60 meters from the Inner-ring Elevated Road (see Figure S1). This field was selected to investigate the main atmospheric transport pathway for anthropogenic emissions from the densely populated and highly urbanized area in the Eastern China. The green space is a typical receptor of urban pollutant emissions, in particular traffic-related emissions. During sampling, local temperature ranged from 3-40°C and average wind speed was <1.5 m s^{-1} with the maximum of 5.5 m s^{-1}.

2.2 Samplers and sampling design.

Commercial 51 μm-thick low-density polyethylene (LDPE) was cut into strips of 40 cm × 10 cm. The strips were cleaned and spiked with performance reference compounds (PRCs, more details in the SI) (Liu et al., 2016). The sharpest

variations in meteorological variables with height occur within the surface roughness layer (< 100 cm above ground in this study). Air samplers were deployed as an array along a gradient of 17 heights from 5 cm to 200 cm above ground, and were fixed non-uniformly at 5, 10, 15, 20, 25, 30, 35, 40, 45, 50, 60, 70, 80, 90, 100, 150, and 200 cm above ground (see Figure S2). To avoid individual samplers blocking each other, they were sequentially distributed in four directions. Meanwhile, three soil samplers (50 cm × 13 cm × 2 cm) were deployed immediately adjacent to the air samplers (< 1 m^2). The soil sampler (a LDPE strip was protected by a metal grid) was vertically inserted into topsoil (<15 cm deep), and stainless steel boxes were placed over the LDPE passive samplers. Seven sampling campaigns of 2 - 8 weeks were performed from Match of 2017 to September of 2018. Detailed information on air/soil samplers and temporal coverage is provided in the SI (see Figures S2-S3 and Table S1).

2.3 Sample analysis and QA/AC.

After sampling, LDPE samples were wiped clean by pure water and hexane to remove the particles and soil dust absorbed on the surface of LDPE strips, and analyzed for PAH concentrations. The LDPE samples were treated according to a method published previously (Liu et al., 2016). Briefly, all LDPE sheets were spiked with surrogate standards (five deuterated PAHs) to assess recovery, and then extracted overnight in dichloromethane and hexane, sequentially. After extracts were concentrated, an injection standard (deuterated fluorene) was added before GCMS analysis. No additional sample cleanup was performed for air samples, while soil samples were passed through a silica gel and sodium sulfate column for cleanup. 16 US EPA PAHs were quantified using an Agilent GC 7890A

with a HP-5 MS fused silica capillary column (30 m × 0.25 mm i.d., 0.25 μm film thickness) equipped with an Agilent 5975C MSD in EI+ selected ion monitoring (SIM) mode. PAH concentrations in LDPE samples were corrected for surrogate standard recoveries and blank-subtracted using field blanks in the same sampling batch. PAH concentrations in field blanks were < 10% of measured concentrations in samples for 3 - 4 rings PAHs, and < 20% for 5 - 6 rings PAHs, except naphthalene (30%) and dibenz [*a,h*] anthracene (47%) (see Table S2). PRC concentrations in field and lab blanks from each batch were used to quantify initial concentrations of PRCs in deployed samples. Measured concentrations in LDPE were used to calculate (equivalent) gaseous concentrations of PAHs in air (or soil) based on LDPE-air partition coefficients corrected to ambient temperature (Liu et al., 2016; McDonough et al., 2014). The calculation is based on the assumption that the uptake rate of target PAHs from ambient environment to the LDPE sheet is equal to the loss rate of PRCs from the LDPE sheet (Booij and Smedes, 2010). Equilibrium percentages of target PAHs were calculated from the quantities of PRCs remaining in each sample. More analytical details and calculations are shown in the Supporting Information (see Tables S2 and S3).

Procedural blanks and field blanks were performed during each campaign to assess the potential contamination for quality assurance. Limits of detection of PAHs were < 1 ng m^{-3} in air and soil air except naphthalene and acenaphthene. Average recoveries of surrogate standards were 45 - 81% and average relative standard deviation percentages of target PAHs were 10 - 25%. Sampling rates were 16 m^3 day^{-1} in air and 4.7 m^3 day^{-1} in soil, respectively. More information on quality assurance and quality control is in the Supporting Information (Tables S1-2 and S4).

2.4 Air-soil diffusive exchange flux of PAHs.

The mass flux ($F_{a/s}$, in ng m^{-2} day^{-1}) is driven by the difference in target's chemical activity between air and soil matrixes, and the Mackay's surface soil fugacity approach was employed for the calculation (Mackay, 2001), see Equation 1.

$$F_{a/s} = \frac{(C_{pe,a} - C_{pe,s})}{K_{PE-a}} \times v_{a/s} \quad (1)$$

where $C_{pe,a}$ and $C_{pe,s}$ are the equilibrium concentrations of PAHs in PE matrix deployed in air and soil, respectively, and $K_{PE\text{-}a}$ is the air temperature-corrected PE-air partition coefficient. Details on estimating overall mass transfer velocity in air-soil diffusive exchange of PAHs ($v_{a/s}$, in m day^{-1}) from the volume fractions of soil water and soil air are provided in the Supporting Information, and the calculated $v_{a/s}$ and $F_{a/s}$ values are presented in Table S5.

2.5 Vertical diffusive flux of PAHs within the air layer.

Both random molecular motion and turbulence promote mixing within the air layer. The vertical diffusive flux (F_{Dual}, in ng m^{-2} day^{-1}) consists of two parts, namely the vertical eddy diffusive flux and the molecular diffusive flux (F_{Eddy} and $F_{mol.}$, in ng m^{-2} day^{-1}). Based on Fick's first law, the mass fluxes are driven by a vertical gradient of PAH concentrations (dC/dH), and related to molecular diffusivity (D_A, in m^2 day^{-1}) and vertical eddy diffusivity (E_z, in m^2 day^{-1}) of PAHs in air, as shown in Equation 2. E_z was estimated only from measured heat fluxes; the contribution of momentum flux was ignored as the horizontal wind vector

was small in this study (< 1.5 m s^{-1}) (Kurt-Karakus et al., 2006; Schwarzenbach et al., 2002). Typically, D_A is around 0.05 cm^2 s^{-1}, while in this study E_z was in the range of 0.01 – 0.6 cm^2 s^{-1} in time-integrated average. Details on estimating the vertical eddy diffusivity and vertical diffusive flux within air phase are provided in the Supporting Information, and the calculated E_z, concentration gradient, and F_{Dual} values are listed in Table S6-S8.

$$F_{Dual} = F_{Eddy} + F_{mol.} = (E_z + D_A)\frac{dC}{dH} \quad (2)$$

2.6 Uncertainty analysis on the calculated fluxes.

Error propagation analysis was applied to estimate uncertainty of the air-soil diffusive exchange flux of PAHs ($F_{a/s}$), errors in PE-air partition coefficients (K_{PE-a}), overall mass transfer velocities ($v_{a/s}$), concentrations of PAHs in PE strips deployed in air and soil ($C_{PE,a}$ and $C_{PE,s}$) were considered, as shown in Equation 3. Five parameters, including vertical eddy diffusivity (E_z), molecular diffusivity in air (D_A), height difference (h), concentration of PAHs at different heights (C_{up} and C_{down}), were included to estimate uncertainty of vertical diffusive fluxes within the air layer (F_{Dual}) in Equation 4.

$$\frac{\delta F_{a/s}}{F_{a/s}} = \sqrt{\left(\frac{\delta K_{PE-a}}{K_{PE-a}}\right)^2 + \frac{\left(\delta C_{PE,a}{}^2 + \delta C_{PE,s}{}^2\right)}{\left(C_{PE,a} - C_{PE,s}\right)^2} + \left(\frac{\delta v_{a/s}}{v_{a/s}}\right)^2} \quad (3)$$

$$\frac{\delta F_{Dual}}{F_{Dual}} = \sqrt{\frac{\left(\delta E_Z{}^2 + \delta D_A{}^2\right)}{(E_Z + D_A)^2} + \frac{\left(\delta C_{up}{}^2 + \delta C_{down}{}^2\right)}{\left(C_{up} - C_{down}\right)^2} + \left(\frac{\delta h}{h}\right)^2} \quad (4)$$

3. RESULTS AND DISCUSSION

3.1 Vertical concentration profiles of gaseous PAHs in air and transport direction of air-soil exchange.

The vertical concentrations of gaseous PAHs on the air side exhibit distinct concentration gradients in space, and directly reveal the transport direction of PAHs. The vertical concentration distributions of PAHs in air are shown exemplary for campaign ADH04 (2017/6/14 - 2017/6/30) in Figure 1. Gaseous concentrations of phenanthrene (see Figure 1.a) increased with the height, from 16 ng m^{-3} at 5 cm to 45 ng m^{-3} at 50 cm above ground, where it remained stable (47 - 51 ng m^{-3}) within the 1 - 2 m. This indicates gas deposition of phenanthrene from an upper air layer to a lower one close to ground. Turbulence also varied with height, which affected both uptake of PAHs and release of PRCs, and in general, the sampling rate increased with height (see Figure 1.f). Gaseous concentrations of phenanthrene have been corrected based on equilibrium percentage of PRCs observed (see Equations S1-S2). The equivalent gaseous concentrations of phenanthrene in topsoil ranged from 1.62 - 2.1 ng m^{-3}, which is significantly ($p < 0.01$) lower than in air (16 - 51 ng m^{-3}). Consequently, transport direction of phenanthrene is confirmed as air-to-soil deposition.

A similar deposition behavior was observed for fluoranthene as shown in Figure 1.b. In contrast, some 4 - 6 rings PAHs showed an unusual volatilization from soil to air, e.g., benzo[*b*]fluoranthene and benzo[*ghi*]perylene (Figure 1.c, d, and e); the spatial trend of chrysene in air was unclear, a possible explanation of which is that chrysene reached or approached equilibrium in air-soil exchange process. The downward deposition of lower molecular weight PAHs (especially phenanthrene) indicates a significant emission in Shanghai urban space and on-

going accumulation of the gaseous PAHs in urban topsoils, whereas the upward volatilization of higher molecular weight PAHs (e.g., 5 - 6 rings PAHs) is different with the general expectation (deposition) and reported observations (Cetin et al., 2017a). We ever suspected the LDPE soil samplers and air samplers at lower heights were more vulnerable to be associated with fine soil dust. In the improved experimental process, the LDPE trips were cleaned up by deionized water and swabbed with a hexane-soaked wiper to ensure that only absorbed molecules into the LDPE samplers would be quantified. Interestingly, passive samplers did 'see' the unusual process. The observed volatilization is possibly attributed to local high legacy pollution or a long-term accumulation from dry and wet deposition (ever-increasing soil fugacity is even greater than the air fugacity) in topsoils and the soil acting as a secondary source of the air PAHs.

In this study, strong linear correlations were obtained by fitting a relationship of gaseous concentration as a function of log-transformed height. Fitted results (solid line) are presented in Figure 1 ($R > 0.68$), which were significantly correlated ($p < 0.01$) for most PAHs except chrysene. Kurt-Karakus et al. (2006) reported a volatilization gradient of DDT in a historically treated agricultural soil in Canada and a similar logarithmic function between height and gas concentration. Wang et al. (2017) observed a deposition gradient of organochlorine pesticides in the pasture of the central Tibetan Plateau, but used a power function to fit the relationship. The curve is related to wind speed (Majewski et al., 1990), or to be more precise, to vertical turbulence. The slopes derived here are further used to quantify vertical concentration gradient at different heights and estimate diffusive flux of PAHs within the air layer (see below). Although different functions were used to fit, interestingly, mathematical

285 expressions are similar based on derivative of the two functions (dC/dH) to
286 describe vertical concentration gradient, e.g., 12.97 H^{-1} for phenanthrene in this
287 study and 4.97 $H^{-0.87}$ for DDT from Wang et al (2017).
288
289 **3.2 Influence of vegetation during the growing season on vertical**
290 **concentration distribution of gaseous PAHs.**
291 Vegetation has been considered as a globally important compartment in
292 scavenging and storing atmospheric pollutants and transferring them into soil
293 through falling litter (Odabasi et al., 2015), or back into the air by re-
294 volatilization (Bao et al., 2016; Terzaghi et al., 2017). Many studies reported
295 urban vegetation as an air pollutant collector based on large scale modeling
296 (Simonich and Hites, 1994; Terzaghi et al., 2017). Furthermore, a lack of
297 experimental investigation has been recognized (Setala et al., 2013). The study
298 here provides an empirical-based evidence on influence of urban vegetation on
299 gaseous PAHs.
300 Vertical distributions of gaseous PAHs before (February), during (March) and
301 after (May - September) the growing season are compared in Figure 2. Gaseous
302 concentrations of phenanthrene, fluoranthene and benzo[*b*]fluoranthene were
303 normalized to a common condition of 25 °C and 1 atm for comparison over time,
304 due to gaseous concentrations of PAHs varying with air temperature and
305 pressure. Field vegetation grew up from ~5 cm height above ground before the
306 growing season to ~30 cm height after the growing season. Overall,
307 concentrations of PAHs decreased over time, e.g. phenanthrene from 50 ng m^{-3} in
308 February to 15 ng m^{-3} in September. This time trend of gaseous PAHs is similar as
309 air pollution in Shanghai (see Figure S3). Clearly, PAH concentrations are linked

to overall air quality, however these vertical patterns of PAHs are similar in different campaigns except B2 (in March), especially for phenanthrene at the heights of 10 - 35 cm in Figure 2.a. The differences of PAH patterns before, during and after growing seasons are attributed to absorption by vegetation during the growing season. For phenanthrene and fluoranthene deposition in the growing season (B2) resulted in markedly lower concentrations in the vegetation layer than in the upper air layer. However, the adsorption by vegetation was not observed after the growing season.

Klingberg et al. (2017) observed substantially lower gaseous PAH levels in parks than adjacent areas near traffic. Ghasemian et al. (2017) reported that the dense canopy improved the near-road air quality. However, the effect remains controversial. Setala's result (2013) suggested a minor capability of urban vegetation to remove air pollutants in northern climates. Moreover, Viippola et al. (2016) and Yli-Pelkonen (2018) reported higher gaseous PAH levels under tree canopies than adjacent open area in southern Finland and northeast China, associating with the trapping of polluted air under canopies and re-volatilization from soil back to the air. Our results support the removal effect of air pollutants by vegetation, but the influence was observable only during the growing season (emergence of new and clean biomass), and the influence faded away after the growing season.

3.3. Air-soil diffusive exchange of PAHs.

Air-soil diffusive exchange is an interphase transfer process, which is usually characterized by the Whitman two-resistance mass transfer coefficient approach (Schwarzenbach et al., 2002). Quantification of the diffusive flux in an air layer

close to the surface by micrometeorological approach is an alternative method. In this study, the micrometeorological approach focused on an air layer with a specific thickness (100 cm), in which air turbulence or eddy diffusion as well as random molecular motion together drive pollutant transfer. In the thin layer close to the air-soil interface, eddies tend to be dampened and movement to and from the interface occurs only by molecular diffusion (Mackay, 2001). Both methods were applied to estimate comprehensively on the air-soil diffusive exchange flux in this study.

3.3.1 Estimation of vertical eddy diffusivity within the air layer close to the air-soil surface.

Molecular diffusivity is commonly isotropic, while eddy diffusivity in the vertical direction is usually much lower than horizontal diffusion (Schwarzenbach et al., 2002). Vertical eddy diffusion can strongly influence PAH transfer in air-soil exchange process. Vertical eddy diffusivity can be calculated from heat and momentum fluxes, more specifically, from temperature profile and horizontal wind vector, respectively (Kurt-Karakus et al., 2006). Due to a lower wind speed in this case, the vertical eddy diffusivity was linked only to the vertical temperature profile close to the surface.

Taking temperature profile within specific three days (including sunny, rainy and cloudy days) for example, the vertical eddy diffusivities (E_z) at the heights of 0 - 5 cm, 5 - 20 cm, 20 - 60 cm, and 60 - 100 cm were calculated from the temperature profile mentioned above, and results are presented in Figure 3. First of all, spatial and temporal variations of air temperature were notable. Especially during sunny days, air temperature varied drastically over time due to solar

radiation, and changed with height above the surface. Moreover, air temperature was much higher than soil temperature during sunny days, while the both temperatures were similar on a rainy day and at nighttime. In addition, vegetation layer was believed to have a significant influence on vertical temperature profile (Daemei et al., 2018). During the deployment period of this study, the height of vegetation layer reached up to ~20 cm above the surface. It was covered by a dense grass layer, meanwhile the temperature difference between soil and air above vegetation in the sunny day was > 10 °C. Consequently, for monitoring real-time temperature profiles in subsequent work, three temperature sensors were deployed in air above vegetation, vegetation layer and soil surface, respectively.

Such temperature profile led inevitably to a great heterogeneity in vertical eddy diffusivity based on the micrometeorological approach, as shown in Figure 3.b. When temperature rose constantly in the morning on a sunny day, air masses warmed up, resulting in an updraft and a negative value of E_z. After temperature reached a peak value at noon, it decreased continually until night and air masses cooled down causing a downdraft and a positive value of E_z. Therefore, vertical eddy diffusion is a vector with a direction (updraft or downdraft). Figure 3.b demonstrates a remarkable variation of eddy diffusivity over time, in magnitude and direction. We calculated the average time-integrated eddy diffusivities of updraft and downdraft, respectively, similar as the E_z values in Figure 4.a and b. Generally speaking, the magnitude of E_z varied with distance to the air-soil surface. The closer to the surface, the smaller E_z value was, and even lower than molecular diffusivity of PAHs in air. The vertical pattern of eddy diffusivity is in line with the above statement that eddy diffusion tends to be damped in a thin

385 layer close to the surface.

386 As a consequence, solar radiation and vegetation cover control temperature
387 vertical profile and finally influence vertical eddy diffusivity in local micro-
388 environment close to ground.

389

390 **3.3.2 Estimation of diffusive flux of gaseous PAHs within the air layer based**
391 **on the micrometeorological approach.**

392 Random molecular motion and vertical eddy motion promote vertical
393 transferring of gaseous PAHs within the air layer close to ground. The diffusive
394 flux, hence, depends on a vertical gradient of PAH concentration (dC/dH), vertical
395 eddy diffusivity (E_z) and molecular diffusivity (D_A) of PAHs in air. The slopes
396 ($dC_{air}/d\ \ln(H)$) in Figure 1 and Table S7 were used to calculate the vertical
397 concentration gradient (dC/dH) at different heights above the surface (see Figure
398 4.a and b). Molecular diffusivity in air is constant at specific condition, e.g. $D_{\mathrm{PhA,A}}$
399 = 0.053 $cm^2\ s^{-1}$for phenanthrene at 25 °C and 1 atm, while vertical eddy
400 diffusivity in air varies with the height above the air-soil surface, as estimated
401 above and shown in Figure 4.a and b. Additionally, the vertical eddy diffusivity is
402 an instantaneous vector with an upward (negative value) or downward (positive)
403 direction. If the direction of vertical eddy diffusivity was the same as the
404 concentration gradient, gaseous PAHs transfer from high to low concentrations. If
405 not, there is no net PAH deposition during an upward eddy flux. In order to
406 estimate the eddy diffusive flux, we calculated the updraft and downdraft eddy
407 diffusivities in time-integrated average during each sampling campaign,
408 respectively (see Table S6). Eddy diffusive fluxes and molecular diffusive fluxes at
409 the heights < 1 m above the surface were calculated (see Table S8) and results of

phenanthrene and benzo[*b*]fluoranthene as examples of deposition and volatilization are shown in Figure 4.

Since phenanthrene deposited from air to soil, the positive eddy diffusivities (downward) were used for calculation, as presented in Figure 4.a. The values of E_z close to the surface (height < 0.1 m) were lower than molecular diffusivity of phenanthrene in air (0.053 $cm^2\ s^{-1}$). With the increase in height, the E_z values increased up to ~0.61 $cm^2\ s^{-1}$ at the height of 1 m, 10 times greater than the molecular diffusivity in air. As for volatilization of benzo[*b*]fluoranthene from soil to air, the negative eddy diffusivities (upward) were used for calculation.

Vertical eddy diffusive flux (F_{Eddy}) and total diffusive flux (F_{Total}=F_{Eddy}+$F_{molecular}$) were estimated based on average updraft/downdraft eddy diffusivity, molecular diffusivity and vertical concentration gradient. The results of phenanthrene and benzo[*b*]fluoranthene are shown in Figure 4.c and d, respectively. In the region close to the air-soil surface (e.g., < 0.1 m), molecular diffusion dominated the mass transfer and percentages of eddy flux to total diffusive flux were < 50% for the two PAHs, as well as uncertainties of the both fluxes were greater than in higher air layer. With increasing distance to the surface, the percentage raised to > 80% at the height > 0.5 m (above vegetation layer).

3.3.3 Estimation of air-soil diffusive exchange flux based on the Mackay's fugacity approach.

To maintain mass balance, the air-soil exchange flux should be equal or similar to the diffusive flux within the air layer. The air-soil exchange fluxes of gaseous PAHs were estimated based on the Mackay's fugacity approach with the Whitman two-resistance model (Mackay, 2001; Schwarzenbach et al., 2002). The exchange

435 flux is related to the concentration difference between two compartments and
436 overall mass transfer velocity of PAHs in air-soil exchange process. The transfer
437 velocity is linked primarily to PAH molecular diffusivities in the atmosphere, soil
438 air and soil water, the boundary layer thicknesses in atmosphere and soil, soil
439 porosity, volume fraction of air and water in soil, soil temperature and Henry's
440 law constant of PAHs. The air-soil exchange transfer velocities and mass fluxes of
441 PAHs are listed in Table S5, and more calculation details in the SI. The mass
442 transfer velocities of PAHs were estimated as 76 - 106 cm day^{-1} in this study.
443 When calculating the air-soil exchange fluxes based on gradients in air and soil
444 fugacities, Tasdemir et al. (2012) placed air sampler on the roof of a building,
445 Donald et al. (2017) deployed passive sampler at the height of ~1.5 m above
446 ground, and Wang et al. (2017) chose the air at 0 - 3 cm above ground to calculate
447 the flux. Since gaseous PAHs levels tended to stable over 50 cm above the surface
448 in this study, air concentrations at the heights of 100 cm and 5 cm were used to
449 calculate the air-soil exchange fluxes (namely F_{100} and F_5, listed in Tables S5),
450 respectively. Taking data from the sampling campaign ADH04 for example, the
451 air-soil exchange fluxes and diffusive fluxes within the air layer were compared in
452 Table 1. For example, for phenanthrene and fluoranthene, the diffusive fluxes
453 within the air layer were 63.2 ng m^{-2} day^{-1} and 3.62 ng m^{-2} day^{-1}, respectively and
454 thus slightly greater than the calculated air-soil exchange fluxes (13.3 - 43.6 ng
455 m^{-2} day^{-1} and 0.19 - 1.62 ng m^{-2} day^{-1}, respectively). While in the soil-to-air
456 volatilization process (e.g. chrysene, benzo[*b*]fluoranthene, and
457 benzo[*ghi*]perylene), the air-soil exchange fluxes were slightly higher than their
458 diffusive fluxes within air layer. But broadly speaking, the two calculated fluxes
459 are comparable based on the two methods, namely the micrometeorological

approach and the Mackay fugacity approach.

In terms of air-soil exchange flux, the values of F_{100} are closer to the diffusive fluxes within air layer in comparison to the F_5 values, but not indicating that F_{100} is recommended. First of all, because of the assumed air boundary thickness of 4.75 mm in the Mackay's fugacity approach (2001), the air concentration should be measured in the air layer as possible as close to the air-soil surface (e.g. 5 cm), and so F_5 would be recommended rather than F_{100}. Second, both of them would be underestimated, but F_{100} is closer to the diffusive flux within air layer due to the greater concentration difference between two compartments. Overall mass transfer velocities ($v_{a/s}$) of gaseous PAHs in air-soil exchange process were estimated based only on their molecular diffusion here. In fact, day-night change (solar radiation) leads to soil temperature variation, which results in different atmospheric boundary layers and different eddy diffusivities of pollutants in air. The calculated transfer velocity, hence, might be underestimated because of the neglect of eddy diffusion in air.

As for air-soil exchange diffusive fluxes in the whole study, observed deposition fluxes were 9.8 ng m^{-2} day^{-1} for fluorene, 31.4 ng m^{-2} day^{-1} for phenanthrene, and 2.5 ng m^{-2} day^{-1} for fluoranthene on average. The other PAHs presented a volatilization flux (e.g. - 0.31 ng m^{-2} day^{-1} for benzo[*b*]fluoranthene) or approached equilibrium (e.g. pyrene and perylene, see Table S5).

4. CONCLUSIONS

In this study, both air-to-soil deposition and soil-to-air volatilization were observed for different PAHs in an urban micro-environment based on their vertical concentration gradients. Concentration-height relationships were

linearized by plotting log-transformed height and gaseous concentrations of PAHs. Influence of vegetation on vertical distribution of PAHs was observable only in the growing season, but insignificant in other seasons. Concentration gradient and micrometeorological condition controlled diffusion of gaseous PAHs. Eddy diffusion dominated the transfer of gaseous PAHs in higher air layer, and was dampened in the layer close to the air-soil surface. Eddy diffusivity was directional and depended mainly on changing vertical profiles of air and soil temperatures. The total diffusive flux within the air layer close to the surface (including vertical eddy diffusive flux and molecular diffusive flux) and air-soil exchange flux based on the Mackay's fugacity approach were comparable to a large extent.

This work demonstrated that monitoring vertical concentrations of gaseous PAHs based on LDPE passive sampling technology is vital to assess transport direction and quantify diffusive fluxes in air-soil exchange process. Although there may be differences in air/soil fugacities between passive and active sampling technologies, passive sampling is a logical choice for better observing vertical concentration distribution with a high spatial resolution and without air disturbance of sampling. Due to its low cost, no power requirement, and easy deployment in air and soil compartments, passive sampling provides a useful tool for monitoring air-soil diffusive exchange process, but field correction for non-equilibrium compounds is needed and yet considerable uncertainties in field measurement are unavoidable.

ASSOCIATED CONTENT

Supporting Information

Detailed information on sampling design and flux calculation can be found along with calculated overall mass transfer velocity, eddy diffusivity, and diffusive flux in the estimated site.

AUTHOR INFORMATION

Corresponding Author.

* E-mail: liu_ying@tongji.edu.cn

Notes

The authors declare no competing financial interest.

ACKNOWLEDGEMENTS

We acknowledge funding from the National Natural Science Foundation of China (No.: 21876126); the Major Science and Technology Program for Water Pollution Control and Treatment of China (No.: 2018ZX07109-001-004), and the Science and Technology Commission of Shanghai Municipality (Nos.:16ZR1438100 and 17DZ1200103).

REFERENCES

Ali, U., Mahmood, A., Syed, J.H., Li, J., Zhang, G., Katsoyiannis, A., Jones, K.C., Malik, R.N., 2015. Assessing the combined influence of TOC and black carbon in soil-air partitioning of PBDEs and DPs from the Indus River Basin, Pakistan. Environmental Pollution 201, 131-140.

Bao, Z., Haberer, C., Maier, U., Beckingham, B., Amos, R.T., Grathwohl, P., 2015. Modeling long-term uptake and re-volatilization of semi-volatile organic compounds (SVOCs) across the soil–atmosphere interface. Science of The Total Environment 538, 789-801.

Bao, Z., Haberer, C.M., Maier, U., Beckingham, B., Amos, R.T., Grathwohl, P., 2016. Modeling short-term concentration fluctuations of semi-volatile pollutants in the soil-plant-atmosphere system. Science of The Total Environment 569-570, 159-167.

Booij, K., Smedes, F., 2010. An improved method for estimating in situ sampling rates of nonpolar passive samplers. Environmental Science & Technology 44, 6789-6794.

Cabrerizo, A., Dachs, J., Barcelo, D., 2009. Development of a Soil Fugacity Sampler for

Determination of Air-Soil Partitioning of Persistent Organic Pollutants under Field Controlled Conditions. Environmental Science & Technology 43, 8257-8263.
Casal, P., Castro-Jimenez, J., Pizarro, M., Katsoyiannis, A., Dachs, J., 2018. Seasonal soil/snow-air exchange of semivolatile organic pollutants at a coastal arctic site (Tromso, 69 degrees N). Science of The Total Environment 636, 1109-1116.
Cetin, B., Ozturk, F., Keles, M., Yurdakul, S., 2017a. PAHs and PCBs in an Eastern Mediterranean megacity, Istanbul: Their spatial and temporal distributions, air-soil exchange and toxicological effects. Environmental Pollution 220, 1322-1332.
Cetin, B., Yurdakul, S., Keles, M., Celik, I., Ozturk, F., Dogan, C., 2017b. Atmospheric concentrations, distributions and air-soil exchange tendencies of PAHs and PCBs in a heavily industrialized area in Kocaeli, Turkey. Chemosphere 183, 69-79.
Cetin, B., Yurdakul, S., Odabasi, M., 2019. Spatio-temporal variations of atmospheric and soil polybrominated diphenyl ethers (PBDEs) in highly industrialized region of Dilovasi. Science of The Total Environment 646, 1164-1171.
Daemei, A.B., Azmoodeh, M., Zamani, Z., Khotbehsara, E.M., 2018. Experimental and simulation studies on the thermal behavior of vertical greenery system for temperature mitigation in urban spaces. Journal of Building Engineering 20, 277-284.
Davie-Martin, C.L., Hageman, K.J., Chin, Y.P., Rouge, V., Fujita, Y., 2015. Influence of Temperature, Relative Humidity, and Soil Properties on the Soil-Air Partitioning of Semivolatile Pesticides: Laboratory Measurements and Predictive Models. Environmental Science & Technology 49, 10431-10439.
Degrendele, C., Audy, O., Hofman, J., Kucerik, J., Kukucka, P., Mulder, M.D., Pribylova, P., Prokes, R., Sanka, M., Schaumann, G.E., Lammel, G., 2016. Diurnal Variations of Air-Soil Exchange of Semivolatile Organic Compounds (PAHs, PCBs, OCPs, and PBDEs) in a Central European Receptor Area. Environmental Science & Technology 50, 4278-4288.
Donald, C.E., Anderson, K.A., 2017. Assessing soil-air partitioning of PAHs and PCBs with a new fugacity passive sampler. Science of The Total Environment 596, 293-302.
Dumanoglu, Y., Gaga, E.O., Gungormus, E., Sofuoglu, S.C., Odabasi, M., 2017. Spatial and seasonal variations, sources, air-soil exchange, and carcinogenic risk assessment for PAHs and PCBs in air and soil of Kutahya, Turkey, the province of thermal power plants. Science of The Total Environment 580, 920-935.
Feng, D.L., Liu, Y., Gao, Y., Zhou, J.X., Zheng, L.R., Qiao, G., Ma, L.M., Lin, Z.F., Grathwohl, P., 2017. Atmospheric bulk deposition of polycyclic aromatic hydrocarbons in Shanghai: Temporal and spatial variation, and global comparison. Environmental Pollution 230, 639-647.
Ghasemian, M., Amini, S., Princevac, M., 2017. The influence of roadside solid and vegetation barriers on near-road air quality. Atmospheric Environment 170, 108-117.
Klingberg, J., Broberg, M., Strandberg, B., Thorsson, P., Pleijel, H., 2017. Influence of urban vegetation on air pollution and noise exposure - A case study in Gothenburg, Sweden. Science of The Total Environment 599, 1728-1739.
Koblizkova, M., Růzickova, P., Cupr, P., Komprda, J., Holoubek, I., Klanova, J., 2009. Soil burdens of persistent organic pollutants: their levels, fate, and risks. Part IV. Quantification of volatilization fluxes of organochlorine pesticides and polychlorinated biphenyls from contaminated soil surfaces. Environmental Science & Technology 43, 3588-3595.
Kurt-Karakus, P.B., Bidleman, T.F., Staebler, R.M., Jones, K.C., 2006. Measurement of DDT fluxes

584 from a historically treated agricultural soil in Canada. Environmental Science & Technology
585 40, 4578-4585.
586 Lammel, G., Klanova, J., Eric, L., Ilic, P., Kohoutek, J., Kovacic, I., 2011. Sources of organochlorine
587 pesticides in air in an urban Mediterranean environment: volatilisation from soil. Journal
588 of Environmental Monitoring 13, 3358-3364.
589 Liu, Y., Gao, Y., Yu, N., Zhang, C., Wang, S., Ma, L., Zhao, J., Lohmann, R., 2015. Particulate matter,
590 gaseous and particulate polycyclic aromatic hydrocarbons (PAHs) in an urban traffic tunnel
591 of China: Emission from on-road vehicles and gas-particle partitioning. Chemosphere 134,
592 52-59.
593 Liu, Y., Wang, S., McDonough, C.A., Khairy, M., Muir, D.C., Helm, P.A., Lohmann, R., 2016. Gaseous
594 and Freely-Dissolved PCBs in the Lower Great Lakes Based on Passive Sampling: Spatial
595 Trends and Air-Water Exchange. Environmental Science & Technology 50, 4932-4939.
596 Mackay, D., 2001. Multimedia environmental models - The fugacity approach, Second ed. Lewis
597 Publishers, Boca Raton.
598 Majewski, M.S., Glotfelty, D.E., Paw, K.T., Seiber, J.N., 1990. A Field Comparison of Several
599 Methods for Measuring Pesticide Evaporation Rates from Soil. Environmental Science &
600 Technology 24, 1490-1497.
601 McDonough, C.A., Khairy, M.A., Muir, D.C., Lohmann, R., 2014. Significance of population
602 centers as sources of gaseous and dissolved PAHs in the lower Great Lakes. Environmental
603 Science & Technology 48, 7789-7797.
604 Odabasi, M., Falay, E.O., Tuna, G., Altiok, H., Kara, M., Dumanoglu, Y., Bayram, A., Tolunay, D.,
605 Elbir, T., 2015. Biomonitoring the Spatial and Historical Variations of Persistent Organic
606 Pollutants (POPs) in an Industrial Region. Environmental Science & Technology 49, 2105-
607 2114.
608 Pokhrel, B., Gong, P., Wang, X.P., Chen, M.K., Wang, C.F., Gao, S.P., 2018. Distribution, sources,
609 and air-soil exchange of OCPs, PCBs and PAHs in urban soils of Nepal. Chemosphere 200,
610 532-541.
611 Qu, C., Albanese, S., Lima, A., Hope, D., Pond, P., Fortelli, A., Romano, N., Cerino, P., Pizzolante, A.,
612 De Vivo, B., 2019. The occurrence of OCPs, PCBs, and PAHs in the soil, air, and bulk
613 deposition of the Naples metropolitan area, southern Italy: Implications for sources and
614 environmental processes. Environment International 124, 89-97.
615 Schwarzenbach, R.P., Gschwend, P.M., Imboden, D.M., 2002. Environmental Organic Chemistry
616 (2nd edition). Wiley Interscience, USA.
617 Setala, H., Viippola, V., Rantalainen, A.L., Pennanen, A., Yli-Pelkonen, V., 2013. Does urban
618 vegetation mitigate air pollution in northern conditions? Environmental Pollution 183,
619 104-112.
620 Simonich, S.L., Hites, R.A., 1994. Importance of Vegetation in Removing Polycyclic Aromatic-
621 Hydrocarbons from the Atmosphere. Nature 370, 49-51.
622 Tasdemir, Y., Salihoglu, G., Salihoglu, N.K., Birgul, A., 2012. Air-soil exchange of PCBs: seasonal
623 variations in levels and fluxes with influence of equilibrium conditions. Environmental
624 Pollution 169, 90-97.
625 Terzaghi, E., Morselli, M., Semplice, M., Cerabolini, B.E.L., Jones, K.C., Freppaz, M., Di Guardo, A.,
626 2017. SoilPlusVeg: An integrated air-plant-litter-soil model to predict organic chemical fate
627 and recycling in forests. Science of The Total Environment 595, 169-177.

Tian, Y., Nie, Z., He, J., Die, Q., Fang, Y., Liu, F., Yang, Y., Gao, X., Huang, Q., 2016. Seasonal variations in concentrations, distributions, and air–soil exchange fluxes of dioxin-like polychlorinated biphenyls in Shanghai, China. Environmental Science and Pollution Research 23, 3376-3384.

Viippola, V., Rantalainen, A.L., Yli-Pelkonen, V., Tervo, P., Setala, H., 2016. Gaseous polycyclic aromatic hydrocarbon concentrations are higher in urban forests than adjacent open areas during summer but not in winter - Exploratory study. Environmental Pollution 208, 233-240.

Wang, C.F., Wang, X.P., Ren, J., Gong, P., Yao, T.D., 2017. Using a passive air sampler to monitor air-soil exchange of organochlorine pesticides in the pasture of the central Tibetan Plateau. Science of The Total Environment 580, 958-965.

Wang, Y., Luo, C.L., Wang, S.R., Liu, J.W., Pan, S.H., Li, J., Ming, L.L., Zhang, G., Li, X.D., 2015. Assessment of the Air-Soil Partitioning of Polycyclic Aromatic Hydrocarbons in a Paddy Field Using a Modified Fugacity Sampler. Environmental Science & Technology 49, 284-291.

Yli-Pelkonen, V., Viippola, V., Rantalainen, A.L., Zheng, J.Q., Setala, H., 2018. The impact of urban trees on concentrations of PAHs and other gaseous air pollutants in Yanji, northeast China. Atmospheric Environment 192, 151-159.

Zhang, Y.Z., Deng, S.X., Liu, Y.A., Shen, G.F., Li, X.Q., Cao, J., Wang, X.L., Reid, B., Tao, S., 2011. A passive air sampler for characterizing the vertical concentration profile of gaseous phase polycyclic aromatic hydrocarbons in near soil surface air. Environmental Pollution 159, 694-699.

Zheng, Q., Nizzetto, L., Liu, X., Borga, K., Starrfelt, J., Li, J., Jiang, Y., Liu, X., Jones, K.C., Zhang, G., 2015. Elevated mobility of persistent organic pollutants in the soil of a tropical rainforest. Environmental Science & Technology 49, 4302-4309.

Zhu, S.Y., Niu, L.L., Aamir, M., Zhou, Y.T., Xu, C., Liu, W.P., 2017. Spatial and seasonal variations in air-soil exchange, enantiomeric signatures and associated health risks of hexachlorocyclohexanes (HCHs) in a megacity Hangzhou in the Yangtze River Delta region, China. Science of The Total Environment 599, 264-272.

FIGURES CAPTIONS

Figure 1. Vertical gas phase concentration profiles of selected PAHs (a - e) and sampling rate (f) at height 5 - 200 cm above ground. (Deployment period: June 14 - 30, 2017)

Figure 2. Effect of vegetation on the vertical gas phase concentration distribution of (a) phenanthrene, (b) fluoranthene and (c) benzo[b]fluoranthene from topsoil to the air layer close to ground in February (B1), March (B2), May (B3), June (B4), July (B5), and September (B7).

Figure 3. Vertical pattern of temperature and eddy diffusivity from topsoil to 1 m height air.

Figure 4. Pattern of vertical eddy diffusivity, concentration gradient, and diffusive fluxes (b) of phenanthrene (PhA) and benzo[*b*]fluoranthene (BbF).

673 Table 1. PAH mass flux [a] (ng m^{-2} day^{-1}) within the air layer close to the ground
674 and in air-soil exchange process.
675

PAHs	Diffusive flux within air layer	Air-soil exchange flux	
		F_{100} [b]	F_5
Phenanthrene	63.2±13.6	43.6±31.6	13.3±9.5
Fluoranthene	3.62±0.76	1.62±1.25	0.19±0.38
Chrysene	-0.17±0.03	-0.39±0.27	-0.39±0.27
Benzo[*b*]fluoranthene	-0.03±0.01	-0.15±0.10	-0.14±0.10
Benzo[*ghi*]perylene	-0.04±0.01	-0.08±0.05	-0.06±0.04

676 [a]: data from the sampling campaign ADH04. Positive values indicate net deposition, while
677 negative values reflect volatilization from soil to air.
678 [b]: F_{100} and F_5 denote fluxes calculated based on the difference of concentrations between the
679 soil surface and the air at a height of 100 cm above ground, and 5 cm above the ground.

680

681

682

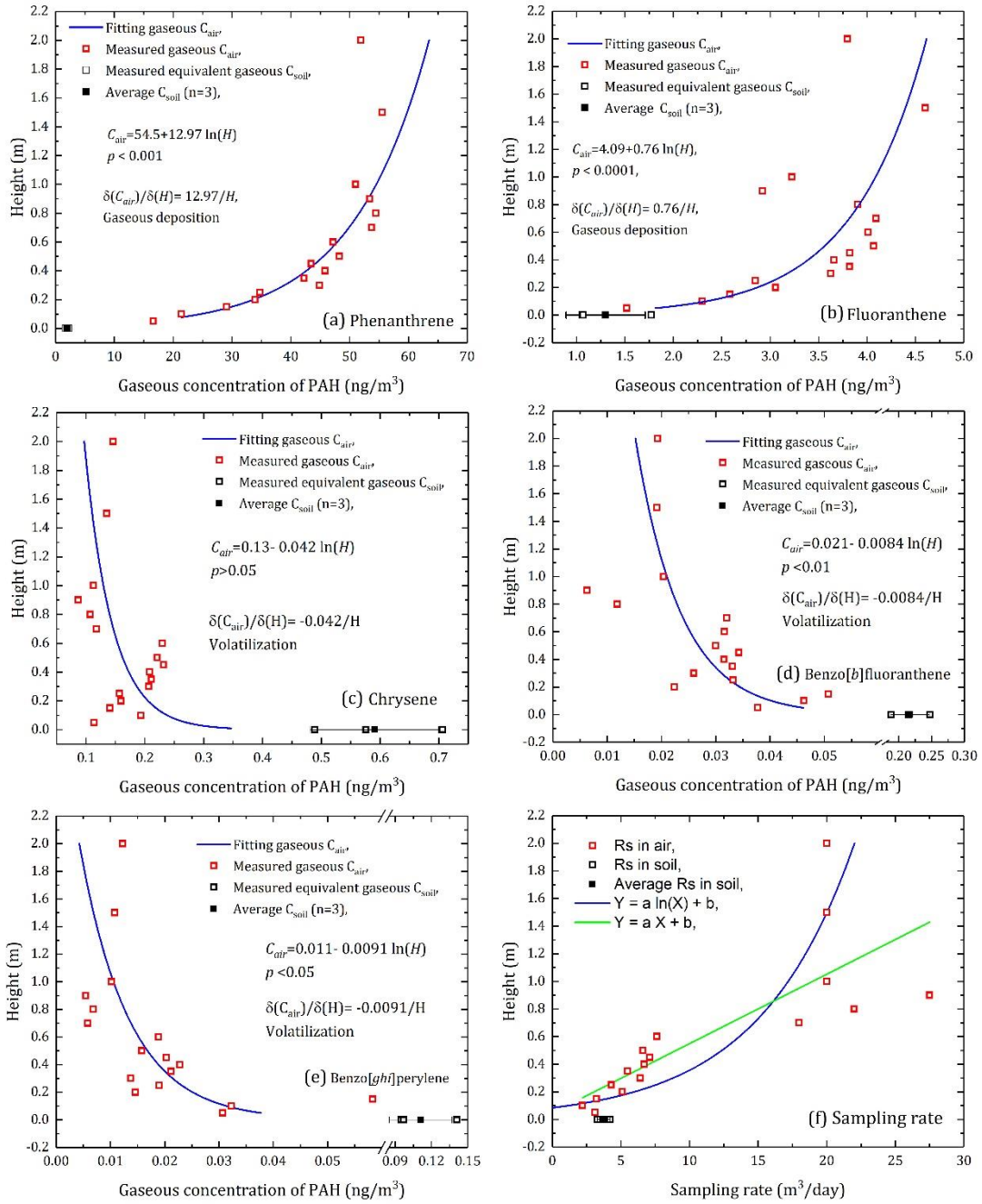

683

684 Figure 1. Vertical gas phase concentration profiles of selected PAHs (a - e) and
685 sampling rates (f) at height 5 - 200 cm above ground. (Deployment period:
686 June 14 - 30, 2017)

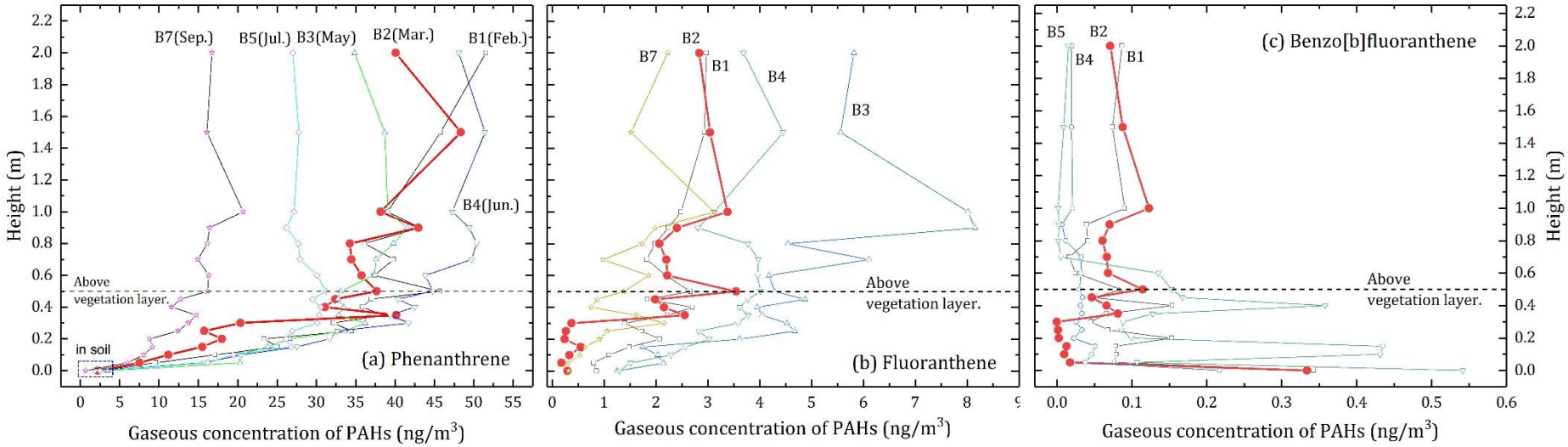

Figure 2. Effect of vegetation on the vertical gas phase concentration distribution of (a) phenanthrene, (b) fluoranthene and (c) benzo[*b*]fluoranthene from topsoil to the air layer close to ground in February (B1), March (B2), May (B3), June (B4), July (B5), and September (B7).

692

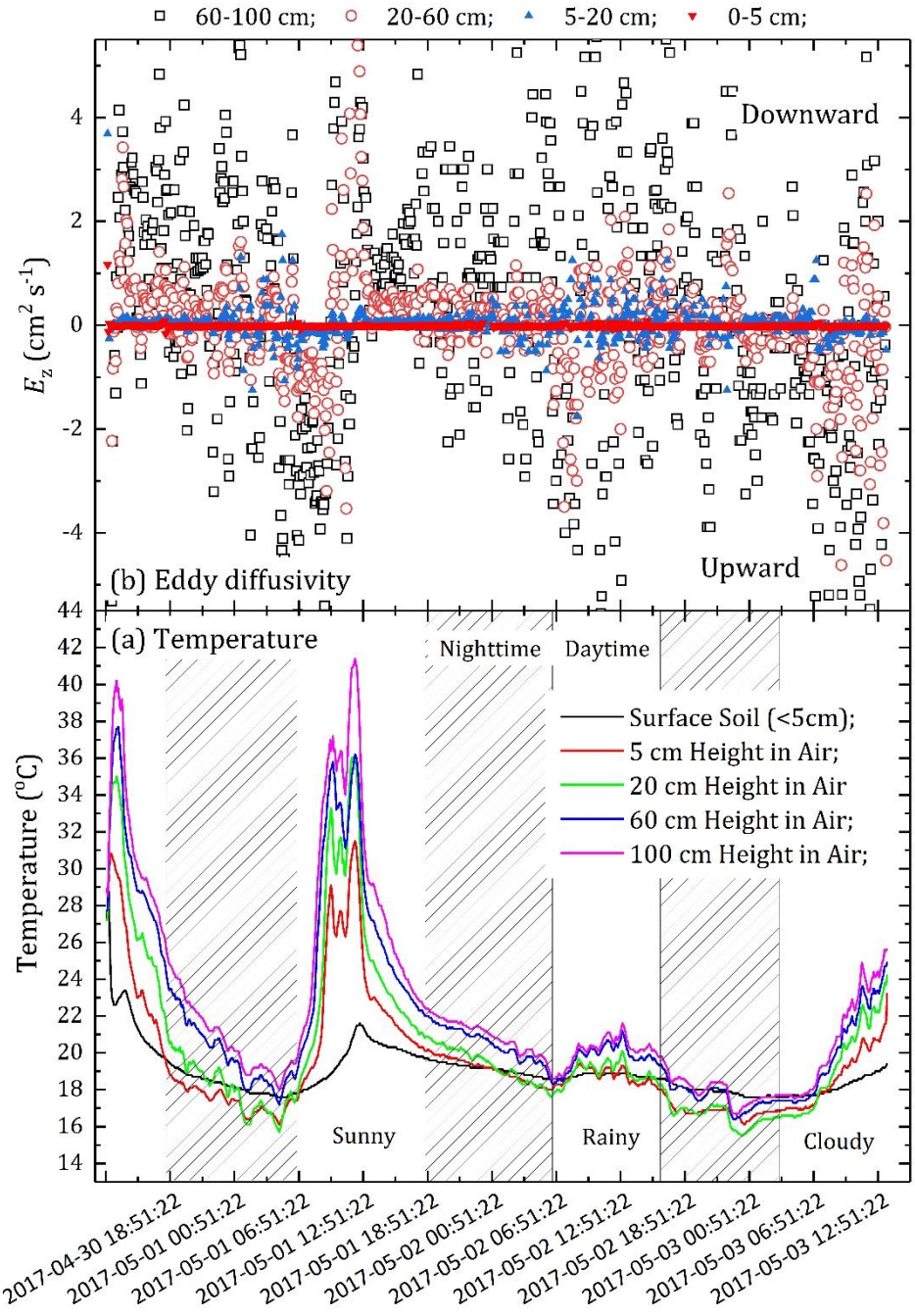

693

694 Figure 3. Vertical pattern of temperature and eddy diffusivity from topsoil to 1 m
695 height air.

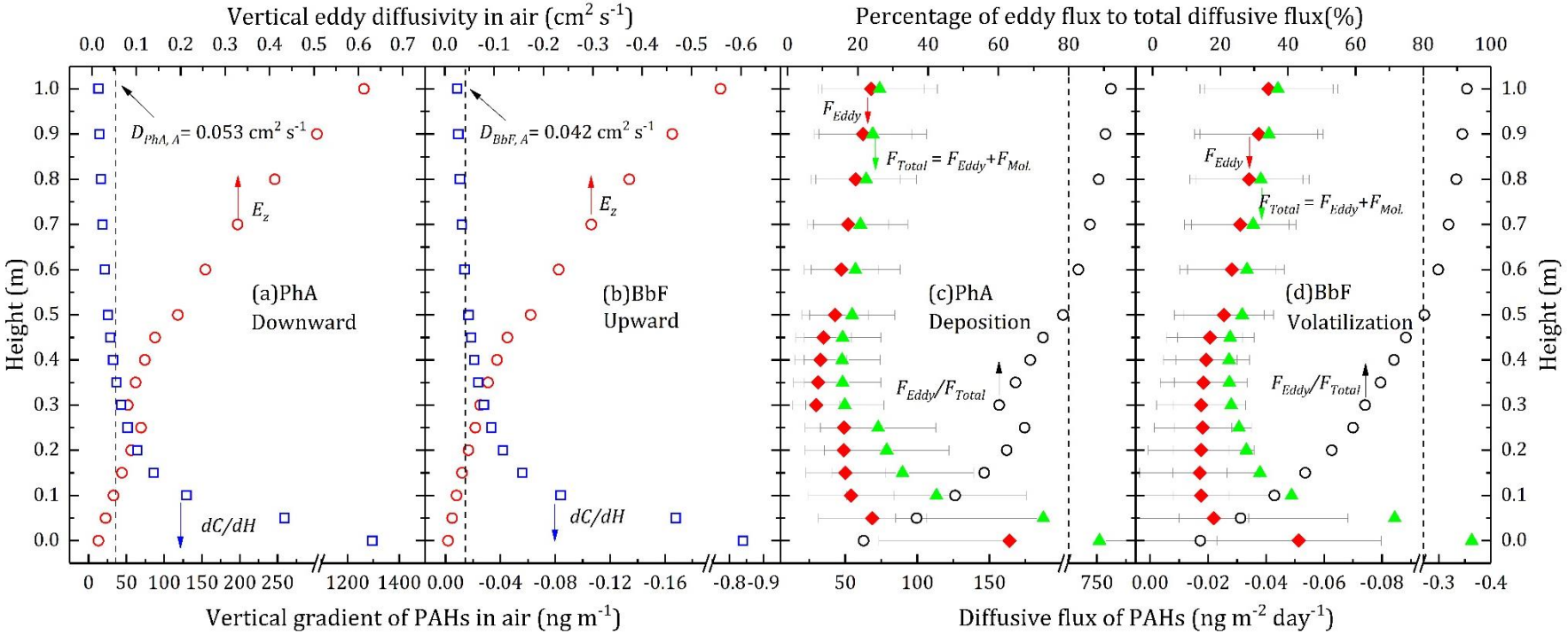

Figure 4. Pattern of vertical eddy diffusivity, concentration gradient, and air diffusive fluxes of phenanthrene (PhA) and benzo[*b*]fluoranthene (BbF).